Earth Planets Space, **51**, 799–807, 1999

Modelling of positively charged aerosols in the polar summer mesopause region

Markus Rapp and Franz-Josef Lübken

Physikalisches Institut der Universität Bonn, Bonn, Germany

(Received August 4, 1998; Revised February 22, 1999; Accepted February 22, 1999)

We present a model based analysis of rocket borne common volume measurements of electron number densities and aerosol charge densities during the ECHO campaign in 1994. During that campaign a sounding rocket was launched into a noctilucent cloud (NLC) as detected by a ground based lidar. At NLC altitudes a particle impact detector gave strong evidence for positively charged aerosols, and an electron probe measured a significant electron enhancement. We have applied a model of aerosol charging to these measurements and find that the existence of positively charged aerosols can be explained if they mainly consist of a substance with a sufficiently low work function. The electron enhancement as well as the aerosol size and number density deduced from our model are consistent with the electron probe and lidar measurements, respectively. Considering the photoelectrical properties of various metals we conclude that only sodium and potassium have a sufficiently low work function to allow for significant photoemission. Even under very favourable conditions the maximum positive charge accumulated on the aerosols is only approximately 4 elementary charges which is much less than discussed in some of the current theories for the creation of polar mesosphere summer echoes. We note that the amount of sodium or potassium required to form these particles is far above the natural abundances at NLC altitudes. The exact abundance and composition of the aerosols need to be known at the time of the in situ measurements in order to make more sophisticated comparisons between measurements and models.

1. Introduction

Aerosols play an important role in the physics of the upper mesosphere region since they give rise to some fascinating and scientifically challenging phenomena, such as noctilucent clouds (NLC), and polar mesospheric summer echoes (PMSE). In the summer season noctilucent clouds are occasionally observed by naked eye soon after sunset at high latitudes. It was realized already at the end of the last century that these clouds are located at approximately 82 km, thus much higher than tropospheric clouds (Jesse, 1891). There is general agreement that NLCs consist of small ice particles which develop by growth and sedimentation starting around the summer mesopause (Turco *et al.*, 1982) where temperatures are as low as 130 K (Lübken, 1999). Once they have arrived at altitudes below ∼82 km, where the atmospheric temperature is typically larger than 150 K, they quickly evaporate.

Very large backscatter signals were first observed with a VHF radar at high latitudes during summer by Ecklund and Balsley (1981) and were later called PMSE. Since they occur only during summer at approximately the same altitudes and geographical latitudes they are presumably closely related to NLCs (see Cho and Röttger, 1997, for a review on PMSE observations and theories). In order to affect the electron number densities, which determine the refractive index for radars in the upper mesosphere, the aerosol particles must be charged. It is commonly believed that they are negatively charged due to electron capture, whereas photoelectrical effects are negligible since most of the solar photons at these altitudes are not energetic enough to overcome the work function of water ice (Reid, 1990; Jensen and Thomas, 1991). In situ observations of electron profiles support this view since they show a steep decrease of electron number densities inside PMSE layers (Ulwick *et al.*, 1988; Lübken *et al.*, 1998). These 'electron biteouts' are believed to be caused by aerosols which scavenge the free electrons and therefore become negatively charged.

The discussion on positively charged aerosols in the high latitude summer mesopause region was stimulated by Havnes *et al.* (1990) who argued that the ice particles leading to PMSEs could be contaminated by metals which have a sufficiently low work function to allow for photoelectrical emission of electrons. This speculation was supported by measurements during the ECHO campaign (in which radar echoes were studied) in 1994 where two sounding rockets were launched to examine the dynamical and electrodynamical conditions in the vicinity of PMSEs. An impact detector called DUSTY was installed to measure the charge state of the aerosols, and the CONE instrument (COmbined Neutral and Electron sensor) measured small scale structures of neutral and electron number densities (Havnes *et al.*, 1996; Lübken, 1996). In one of the rocket flights DUSTY indeed showed strong indications for positively charged aerosols, and CONE measured an electron density enhancement relative to a smooth background (Blix *et al.*, 1995; Havnes *et al.*, 1996). In addition, a ground based lidar located very close to the rocket launch site detected a NLC layer at exactly the same altitudes (Lübken *et al.*, 1996). In this paper we make

an attempt to explain these observations in terms of aerosol charging. We have therefore extended the aerosol charging model of Jensen and Thomas (1991) by explicitly taking into account the role of photoelectrical emission of electrons for the case that the aerosols mainly consist of metals. Our model results are relevant beyond the application to these measurements since we will derive more general results (e.g., the maximum possible positive charge on aerosols) which are of interest for current PMSE theories.

In Section 2 we will shortly recall the basics of the aerosol charging model and discuss our extensions, whereas in Section 3 we will apply the model to the data of the ECHO flight labeled ECT07, as well as the corresponding lidar measurements. We will derive aerosol properties, e.g. mean charge and radius, which are consistent with the ground based and in situ measurements. In Section 4 we will discuss the assumptions made in Section 3 and we will speculate about the constraints imposed by the optical properties of the aerosol particles on their composition.

2. Charging of Aerosols

2.1 The charging model

The model of Jensen and Thomas (1991) determines the charge distribution on aerosol particles due to charge fluxes onto and away from the aerosol. The main idea is to calculate the charge flux balance on q-fold charged particles under steady state conditions which is expressed in a recursion relation first derived by Parthasarathy (1976):

$$P_q \nu_\mathrm{p} + P_q \nu_q^+ n_\mathrm{i} + P_q \nu_q^- n_\mathrm{e} = P_{q+1} \nu_{q+1}^- n_\mathrm{e} + P_{q-1} \nu_{q-1}^+ n_\mathrm{i} + P_{q-1} \nu_\mathrm{p}. \quad (1)$$

Here, $P_q(r)$ represents the number density of particles with fixed radius r which have accumulated a number of q elementary charges (note that $\sum_q P_q(r) = N_\mathrm{A}(r)$, where $N_\mathrm{A}(r)$ is the total number density of aerosols with radius r); ν_p is the photoemission rate; ν_q^+ and ν_q^- are the capture rates of positive ions and electrons, respectively, by a q-fold charged aerosol; n_i and n_e are the number densities of positive ions and free electrons, respectively, in the volume considered. The left hand side of Eq. (1) represents all loss mechanisms for q-fold charged particles (namely photoemission, positive ion capture and electron capture of a q-fold charged particle), whereas the right hand side expresses their sources: electron capture of a $(q+1)$-fold charged particle, and positive ion capture and photoemission of a $(q-1)$-fold charged particle. In our model we allow the aerosols to accumulate a maximum of 8 negative and 500 positive elementary charges, respectively ($q \in [-8, +500]$). The latter quantity is a significant extension of the model of Jensen and Thomas (1991) which took into account a maximum of 4 positive charges which restricts the model to aerosol particles consisting of a material with negligible photoemission, e.g. of pure water ice.

The capture rates of electrons and positive ions ($\nu_q^{-/+}$) contributing to the charge probability distribution $P_q(r)$ have been given by Natanson (1960) and slightly modified by Parthasarathy (1976) applying basic laws of gas kinetics and electrostatics. In our model the crucial quantity is the photoemission rate ν_p which is given by (Turco *et al.*, 1982):

$$\nu_\mathrm{p} = \pi r^2 \int_{100\ \mathrm{nm}}^{\lambda_\Phi} Q_\mathrm{abs}(r, m(\lambda)) \cdot F(\lambda) \cdot Y(\lambda) \cdot d\lambda. \quad (2)$$

Here $Q_\mathrm{abs}(r, m(\lambda))$ is the Mie absorption efficiency, $m(\lambda) = n(\lambda) + ik(\lambda)$ is the complex index of refraction for the aerosol particle under consideration, $F(\lambda)$ is the solar flux, and $Y(\lambda)$ is the photoelectric yield. The integration limits are given by the solar spectrum which is very weak at wavelengths below 100 nm, and by the wavelength λ_Φ which corresponds to the energy of the work function Φ for the aerosol. If the aerosol particles consist of water ice with $\Phi = 8.7$ eV the Ly_α line in the solar spectrum constitutes the main contribution to the integral in Eq. (2). In this case we find that $\nu_\mathrm{p} \ll \nu_q^{+/-} n_\mathrm{i/e}$, i.e., photoeffect can be neglected, in agreement with other studies.

The situation is entirely different if the aerosols consist at least partly of substances with sufficiently low work functions to allow for substantial photoemission. We will now evaluate the photoemission rates for various elements applying Eq. (2). We have taken the complex refractive index as a function of wavelength $m(\lambda)$ for various metals being relevant in the upper mesosphere from Hellwege and Hellwege (1962), and the solar spectrum $F(\lambda)$ from Brasseur and Simon (1981). For the photoelectrical yield $Y(\lambda)$ we have applied the Fowler-Nordheim law following Feuerbacher and Fitton (1972):

$$Y = C(\Phi - h\nu)^2. \quad (3)$$

Here Φ is the work function, $h\nu$ is the quantum energy of the incoming photon, and C is a constant which is taken from measurements. We note that Y depends on Φ and thus on the substance under consideration. Typical values of C are $10^{-2}/(\mathrm{eV})^2$ to $10^{-4}/(\mathrm{eV})^2$ depending on both the size and the composition of the particle (Schmitt-Ott *et al.*, 1980). The Fowler-Nordheim law is not dependent on temperature, except for wavelengths very close to the threshold Φ (see equations 8–10 in Fowler, 1931) which is not of importance for our application. We have chosen rather large values for C relevant for particle sizes comparable to or even smaller than the mean free path of the photoelectrons in the material ($\lesssim$50 nm) in which case electrons from the bulk of the particle are emitted while for bigger particles only the surface of the particle contributes to photoemission (Schmitt-Ott *et al.*, 1980; Müller *et al.*, 1988, 1991). Some measurements of C stated above were performed in pure helium and gave yields which are significantly different from those in a mixture of nitrogen and oxygen (Müller *et al.*, 1988). We prefer to use the measurements in a gas mixture of N_2 and O_2, i.e., approximate of the composition in the upper atmosphere, and have taken the large value of $C = 0.01/(\mathrm{eV})^2$ from Schmitt-Ott *et al.* (1980) since we want to arrive at an upper estimate of the quantum yield.

In Fig. 1 we have plotted the photoemission rate from a single aerosol particle as a function of wavelength assuming a fixed particle radius of 50 nm. We have chosen various metals of interest in the upper mesosphere, and for comparison water ice. We have also plotted the solar irradiance spectrum in Fig. 1. As can be seen from this plot the largest

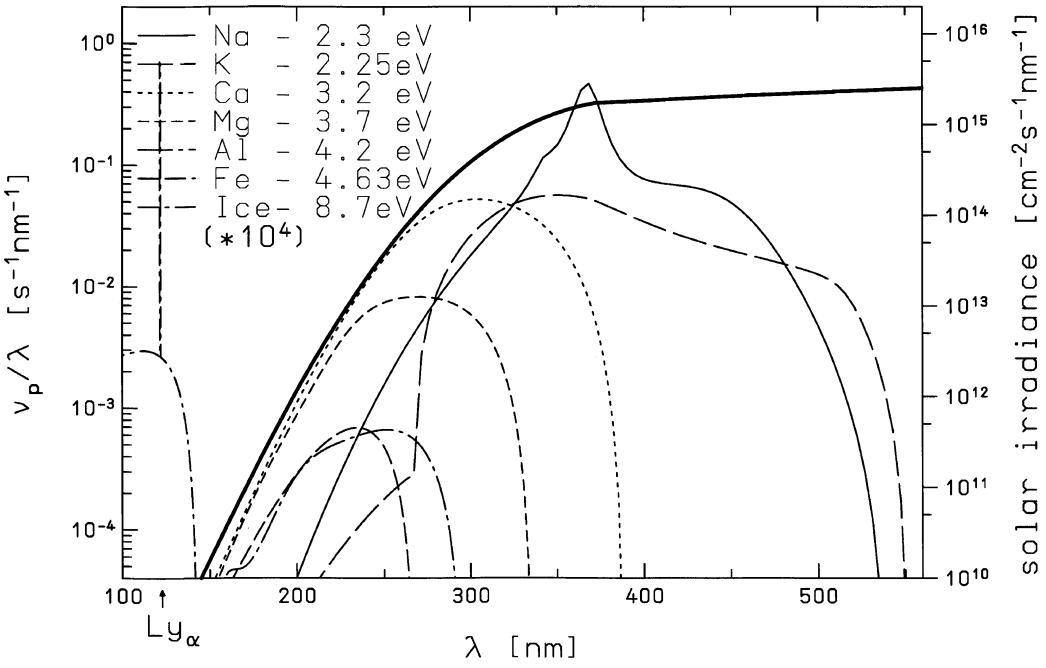

Fig. 1. Photoemission rates per wavelength (thin lines) of a single aerosol particle as a function of wavelength assuming that the particle has a radius of 50 nm. The various elements and their work functions are indicated in the plot. The solar spectrum (thick solid line, right axis) determines the photoemission rates at low wavelengths, whereas the various work functions lead to the cut off at larger wavelengths. For comparison the photoemission rate of a water ice particle is also plotted (note that this curve has been multiplied by 10^4). The wavelength of the Ly$_\alpha$ line in the solar spectrum is indicated.

photoemission rates are expected if the particle consists of sodium. Photoemission rates get very small for λ smaller than ∼250 nm due to the very weak solar spectrum. At the upper wavelength part the photoemission rate is limited by the work function. Note that the photoemission rate of water ice is several orders of magnitude smaller compared to the metals (for plotting reasons the corresponding curve in Fig. 1 has been multiplied by 10^4). In order to obtain the total photoemission rate the curves in Fig. 1 have to be integrated over the wavelength range of interest. The corresponding numbers are listed in Table 1. The photoemission rate for sodium particles is the largest and more than 5 orders of magnitude larger compared to water ice.

Applying the photoemission rate calculations presented above we determine the charge distribution as follows: We start with an initial guess for the electron and positive ion densities assuming that aerosols do not affect these densities (we have ignored negative ions since they are not of significant abundance during daytime conditions). For a given aerosol number density and size we then calculate the aerosol charge distribution $P_q(r)$ from Eq. (1). From $P_q(r)$ and the aerosol number density the number of free electrons and ions being transferred (per second) to the aerosols is calculated assuming steady state conditions and taking into account the requirement of charge neutrality $n_i + z_p = n_e$, where z_p is the total aerosol charge (see Jensen and Thomas, 1991, for more details). This results in modified electron and ion densities which are then used to again determine $P_q(r)$. This procedure is repeated until the values for n_e and n_i converge. The condition for convergence is that the plasma densities calculated in the nth step of the iterative process do not deviate from the $(n-1)$st step by more than 0.1 per mille.

Table 1. Emission rates of photoelectrons of a single particle with a radius of 50 nm for various metals relevant for the mesopause region.

Substance	ν_p (1/s)
Na	18.8
K	7.4
Ca	4.6
Fe	0.036
Mg	0.67
Al	0.048
Ice	4.4×10^{-5}

Please note that for all our calculations we have assumed steady state. We are confident that this assumption is reasonable since typical timescales for the charging mechanisms are 25 s and 0.1 s for a particle with a radius of $r_A = 5$ nm and $r_A = 50$ nm, respectively (see below and Fig. 4), and typical timescales for transport are on the order of hours.

In order to investigate the effect of photoemission on the overall charge of the aerosols we have to make an assumption about the aerosol composition, more precisely about the complex refractive index as a function of wavelength in the relevant part of the solar spectrum. We will later discuss

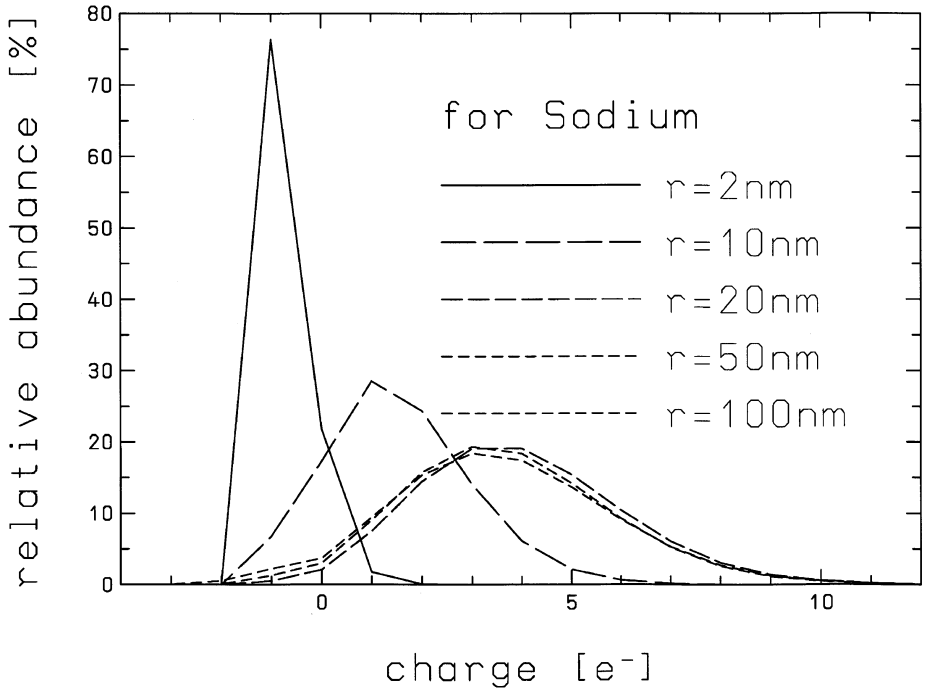

Fig. 2. Aerosol charge distribution assuming that the particles consist of sodium. While small particles (e.g., $r = 2$ nm) are negatively charged, large particles accumulate a net positive charge. The mean maximum positive charge approaches an upper limit of $\sim +4$ e for radii larger than $\sim$20 nm.

in detail various materials in question and their abundance in the upper mesosphere. In the next section we will start with the most promising though probably unrealistic case, i.e., particles that entirely consist of sodium.

2.2 Charging studies for sodium particles

We now apply the charging model described above to particles which entirely consist of sodium, since the photoemission rate is largest for this substance (see Fig. 1 and Table 1). As described above we have used $C = 0.01/(\mathrm{eV})^2$ which results in the maximum possible positive charge. Figure 2 shows the charge distribution on sodium particles with various radii. While very small particles with $r \sim 2$ nm are negatively charged, particles with $r = 10$ nm accumulate a mean positive charge of $\sim +1$ e. It is interesting to note that the mean positive charge reaches a maximum of approximately +(3–4) e for radii larger than $\sim$20 nm and does not further increase with increasing radius. This is in contrast to the results of Havnes *et al.* (1990) who found that the positive charge rises proportional to the aerosol radius. Since this discrepancy has important consequences for some PMSE theories we will now study in detail the physical reasons for a maximum in the aerosol charge.

We first analyze the radial dependence of the photoemission rate in Eq. (2) which is given by $\pi r^2 Q_{\mathrm{abs}}(r, \lambda) \equiv \sigma_{\mathrm{abs}}$ (σ_{abs} is the absorption cross section). We fix the wavelength at 370 nm since the photoemission rate peaks around this wavelength (see Fig. 1). In Fig. 3 we have plotted the radial dependence of the Mie cross sections for absorption, extinction, and scattering. As can be seen from this figure the absorption cross section is proportional to r^3 (thus to the volume of the particle) for particles with radii smaller than $\sim$10 nm (e.g., much smaller than the wavelength), and the scattering cross section is proportional to r^6. This is the classical result for Rayleigh scattering (van de Hulst, 1981). However, for large particles ($r \geq 1000$ nm) the absorption is proportional to r^2 thus to the particle surface. For intermediate sized particles the cross section varies approximately with r^1 with significant interference structures overlayed.

To further elucidate the charge distribution shown in Fig. 2 we have plotted the radial dependence of the various contributions to the charge balance, i.e. the photoemission rate, the capture rate of electrons by neutral particles, and the capture rate of electrons by one to tenfold positively charged aerosols in Fig. 4. We start our discussion with very small neutral particles. As can be seen from Fig. 4 the electron capture rate by a neutral particle smaller than $\sim$5 nm is larger than the photoemission rate resulting in a net negative charge. As the particle size increases the photoemission rate increases proportional to r^3 compared to the approximate r^2 increase of the electron capture rate. This implies that particles of e.g. 6 nm emit more photoelectrons than they capture from the environment which results in a net positive charge. For particles with a radius of $\sim$7.5 nm (12 nm, 15 nm) the photoemission rate is compensated for by electron capture by a singly (twofold, threefold) positively charged aerosol. For particles larger than $\sim$20 nm the radial dependence of the photoemission rate flattens to $\sim r^1$ and reaches equilibrium with the electron capture rate by a fourfold positively charged aerosol. This explains why the particles accumulate not more than 4 positive charges, even if they are significantly larger than 20 nm (this is true as long as the particles are smaller than $\sim$1000 nm when the radial dependence of photoemission changes again; since NLC particles are much smaller than 1000 nm we will not study this case any further). Havnes *et al.* (1990) have

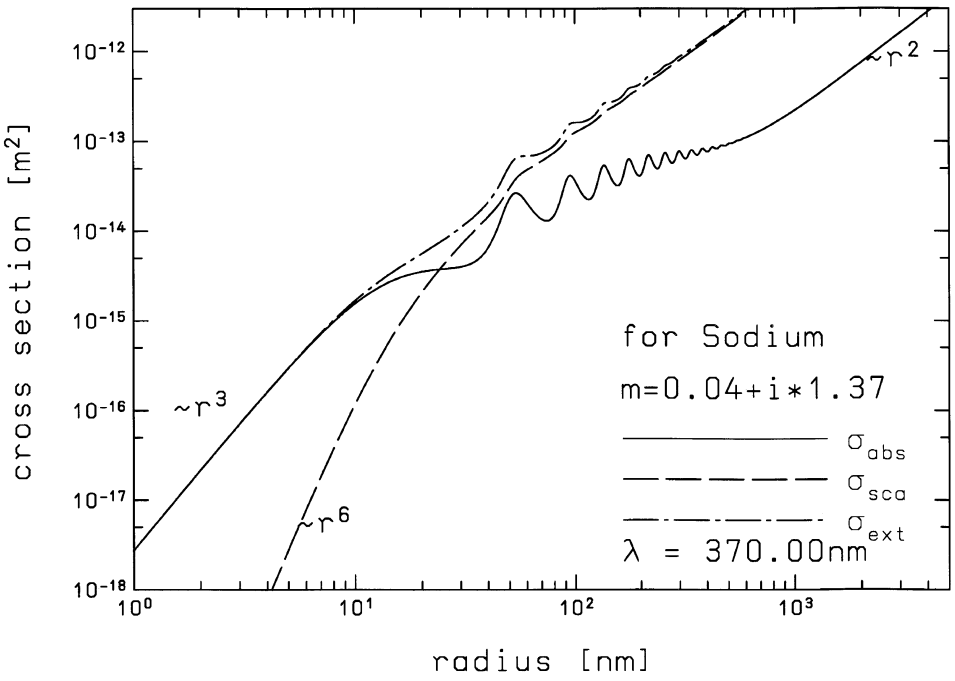

Fig. 3. Radial dependences of Mie cross sections for absorption, scattering, and extinction as a function of particle radius for a wavelength of 370 nm. For particles smaller than ∼10 nm the absorption cross section is proportional to the volume of the particle, and for particles larger than 1000 nm it is proportional to its surface. In between, there is a smooth transition with an approximate r^1 dependence and interference patterns overlayed.

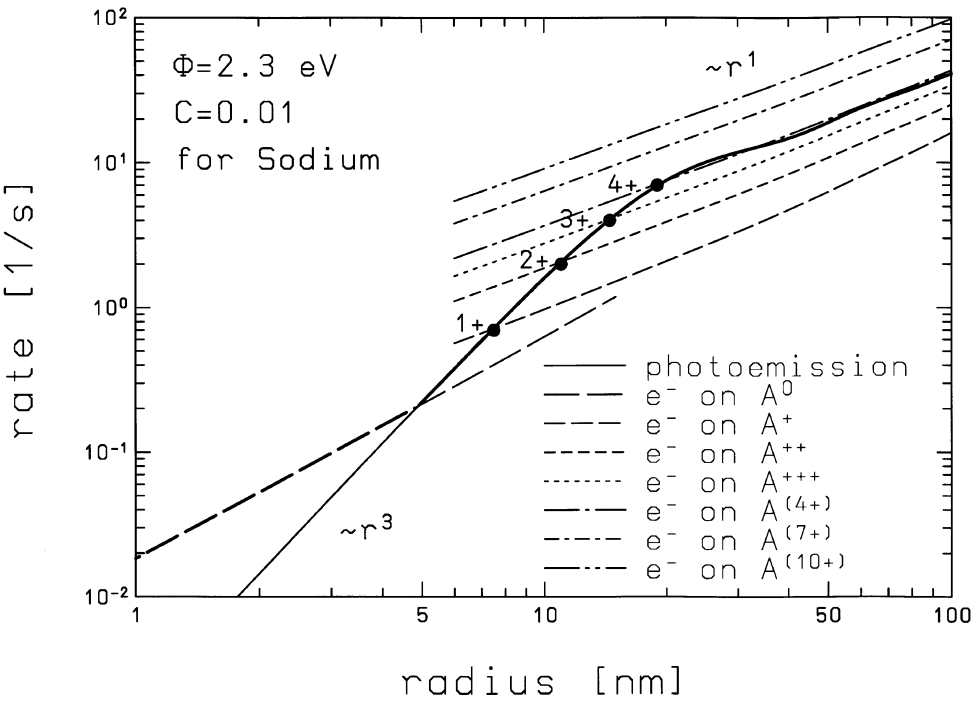

Fig. 4. Photoemission rate (solid line), and capture rates of electrons by neutral (A^o), singly (A^+), and multiply (up to tenfold) positively charged aerosols (see legend). The thick solid line indicates the photoemission rate in equilibrium with the electron capture rate of the positively charged aerosols. For particles with a radius of ∼7.5 nm (12 nm, 15 nm) the photoemission rate is compensated for by electron capture by a singly (twofold, threefold) positively charged aerosol (large dots). For particles smaller than ∼5 nm charging is dominated by electron capture by neutral particles (thick dashed line). For radii larger than ∼20 nm the photoemission rate is compensated for by the capture of electrons by fourfold positively charged aerosols. The model calculations were performed for particles with a work function of $\Phi = 2.3$ eV, and $C = 0.01/(\text{eV})^2$ in Eq. (3).

Table 2. Work functions and maximum positive charge $\bar{q}_{\max}$ of various metals relevant for the mesopause region. The maximum charges have been calculated assuming that the particles are pure metallic, and that they are not larger than ∼1000 nm.

Substance	Φ (eV)	$\bar{q}_{\max}$ (e)
Na	2.3	3.8
K	2.25	∼2
Fe	4.63	≤0
Ca	3.2	≤0
Mg	3.7	≤0
Al	4.2	≤0

used an absorption cross section which is proportional to r^3 for all wavelengths smaller than 300 nm. This results in too large photoemission rates, and in too large positive charges for particles larger than ∼20 nm and explains the discrepancy mentioned above.

2.3 Sensitivity studies

We have studied the influence of the optical properties of the aerosol particles (i.e., the model parameters C, Φ, and the refractive index) on the maximum positive charge $q_{\max}$ accumulated on the aerosols with radii larger than ∼20 nm. We have already noted that $q_{\max} \sim +3.8$ e for sodium. For simplicity we have assumed that the particles consist of pure K, Ca, Fe, Mg, and Al, respectively. We have adapted the work function energies from Weast (1978), the refractive indices from Hellwege and Hellwege (1962), and have again used $C = 0.01/(\text{eV})^2$. The results of these calculations are summarized in Table 2. It is evident that most of the elements have too large work functions to allow for a positive charging of the aerosols. Only sodium and potassium particles would accumulate approximately 3.8 and ∼2 positive charges, respectively. Despite the fact that the work functions of both Na and K are almost identical the maximum charge differs by almost a factor of 2 due to the quite different variation of the complex refractive index with wavelength for both metals.

We have also varied the constant C within reasonable limits and found that $\bar{q}_{\max}$ is approximately proportional to C: Decreasing C by a factor of 10 decreases $\bar{q}_{\max}$ by the same factor.

3. Application of the Aerosol Charging Model to Flight ECT07

We will now apply the charging model to measurements performed during a sounding rocket flight labeled ECT07. This flight took place from the Andøya Rocket Range (69°N) on July 31, 1994, at 00:50:33 UT as part of the ECHO campaign. The DUSTY instrument on board the sounding rocket measured strong signals at exactly the altitude range where the Bonn University lidar detected a strong backscatter ratio of $R \sim 100$ indicative of a NLC layer (Lübken *et al.*, 1996). In addition, a VHF radar received strong PMSE signals from these altitudes (Nussbaumer *et al.*, 1996). Post flight analysis lead Havnes *et al.* (1996) to conclude that DUSTY had detected positively charged aerosols with a maximum charge density of $N_A \cdot q_A \sim 7000$ e/cm^3 at an altitude of 83 km (q_A is the mean aerosol charge). As has been stated by Havnes *et al.* (1996) the absolute value for $N_A \cdot q_A$ is somewhat questionable due to unknown instrumental effects. At exactly the altitude range where DUSTY detected charged aerosols, the electron probe of the CONE instrument measured a significant free electron density enhancement of $\Delta n_e \sim 3000$ e$^-$/cm^3 on top of a smooth background profile (Blix *et al.*, 1995). In addition, a 'falling sphere' was launched close in time and space to the sounding rocket and gave atmospheric density and temperature profiles below ∼95 km altitude. These temperatures have been used in our model to calculate the capture rates.

This set of measurements provides the unique possibility to test the aerosol charging model and investigate whether we arrive at a solution which is consistent with all measurements. We can then study the implications of the results for our understanding of the aerosol composition and the role of charged aerosols in creating PMSE.

We start with the lidar result ($R = 100$) and show in Fig. 5 backscatter ratios as a function of aerosol radius and number density; more precisely, the mode radius of a lognormal aerosol size distribution with a moderate width of $\sigma = 1.2$ following Thomas and McKay (1985) is used on the abscissa in Fig. 5. As can be seen from this plot a backscatter ratio of 100 requires that the particles are larger than ∼25 nm, assuming reasonable number densities of not more than several thousand particles per cm^3. From our model calculations we conclude that particles of this size carry a positive charge of $q_A = +3.8$ e (assuming that the particles consist of sodium; see Fig. 2). Please note that this result is not sensitive to the special choice of σ since for radii larger than 20 nm the particle charge distribution is independent of the particle radius (see Fig. 2). Together with the DUSTY measurement of $N_A \cdot q_A \sim 7000$ e/cm^3 this implies that the aerosol number density is ∼1800/cm^3. Again referring to Fig. 5 this results in a more precise estimate for the mode radius of ∼30 nm. The calculations are summarized in Table 3. With these results we now run the charging model to determine the electron number density enhancement $\Delta n_e = n_{e,\text{disturbed}} - n_{e,\text{undisturbed}}$ using an undisturbed electron number density of ∼3100 e/cm^3 (Blix *et al.*, 1995) which is in agreement with an electron/ion production coefficient of 10 cm^{-3}s^{-1} and a recombination coefficient of 10^{-6} cm^{3}s^{-1} (Jensen and Thomas, 1991). In Fig. 6 we have plotted isolines of Δn_e as a function of the particle mode radius, and the aerosol number density. As can be seen from this figure the aerosol particles must be larger than ∼6 nm in order to produce an electron enhancement, otherwise an electron depletion will occur. This is consistent with our analysis presented in Fig. 4. For a mode radius of 30 nm and an aerosol number density of 1800/cm^3 we expect an electron enhancement of ∼2000 cm^{-3}. This is in reasonable agreement with the measured value (∼3000 cm^{-3}) taking into account the various uncertainties of the model parameters and the measurements. It is interesting to note that the same aerosol population would have resulted in an electron biteout of about −2500 cm^{-3} (rather than the observed enhancement) if the particles are assumed to consist of ice.

We conclude that our model is capable of explaining the

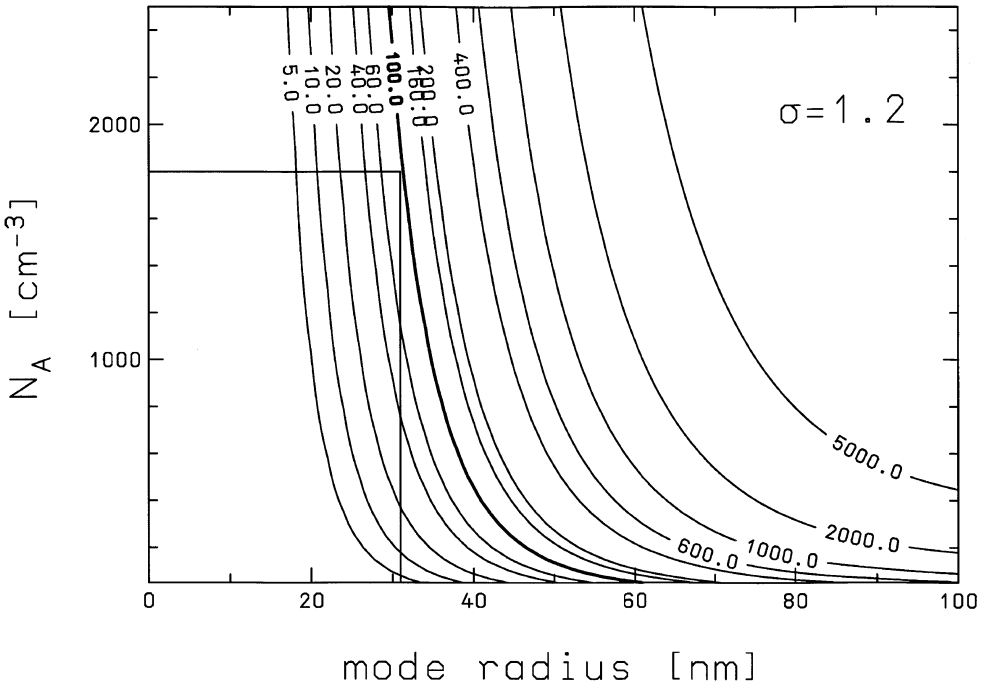

Fig. 5. Lidar backscatter ratio for a wavelength of 532 nm as a function of aerosol number density N_A and mode radius (the width of the lognormal distribution was assumed to be $\sigma = 1.2$). The observed backscatter ratio of ~100 implies that the aerosols must be larger than ~25 nm, assuming that the particle number density is within reasonable limits of several thousand/cm^3.

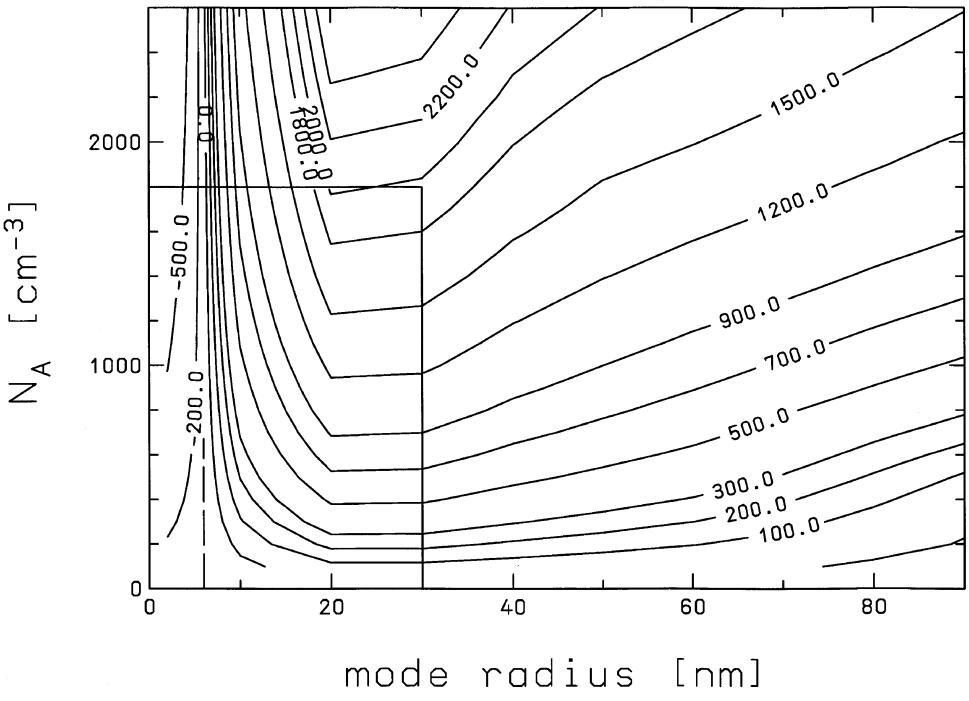

Fig. 6. Model calculation of electron density enhancement in cm^{-3} as a function of aerosol number density N_A and mode radius (the width of the lognormal distribution was assumed to be $\sigma = 1.2$). The aerosols must be larger than ~10 nm to create a positive electron density disturbance. From the lidar and aerosol measurements combined with the model calculations of the aerosol charge distribution we arrive at an aerosol number density of 1800/cm^3, and a mode radius of 30 nm. Applying our model this results in an electron density enhancement of ~2000/cm^3 in good agreement with the in situ measurement.

Table 3. Measurements and model results for ECHO flight labeled ECT07. N_A is the aerosol number density, q_A their mean charge, and r_A their mode radius; n_e is the undisturbed electron number density (see text for more details).

$N_A \cdot q_A$ (e/cm^3)	n_e (cm^{-3})	N_A (cm^{-3})	q_A (e)	r_A (nm)
7000	3100	1800	3.8	30

measurements of DUSTY and CONE in terms of 3.8-fold positively charged aerosols. The size and number density of the aerosols are consistent with the observed lidar backscatter ratio. The most questionable assumption made in our model calculation regards the composition of the aerosols which we have taken to be pure sodium. We will discuss the implications of this assumption in the next section.

4. Discussion

We have demonstrated in the previous sections that aerosols consisting of sodium would result in a positive charge which explains the in situ plasma density measurements and the ground based lidar observations. Potassium particles would also be positively charged, whereas all other metals, e.g. Mg or Fe, and of course ice which is commonly believed to form these particles, have too large work functions to allow for significant emission of photoelectrons. We will now discuss whether there are enough sodium or potassium atoms available at mesopause heights to form such aerosols, or at least to cover their surface with a monolayer. Since the abundance of potassium is an order of magnitude smaller compared to sodium (von Zahn and Höffner, 1996) we will concentrate on sodium.

Resonance lidar measurements have shown that the maximum abundance of free sodium atoms around 85 km is of the order of 10^4/cm^3, and much smaller during summer conditions (e.g. Kurzawa and von Zahn, 1990). Even if we take into account the sodium atoms stored in various chemical substances the total abundance will not increase significantly. Since the radius of a sodium atom is $\sim$0.2 nm at least 30000 atoms are needed to cover the surface of a 30 nm particle, which corresponds to a total of $3 \cdot 10^7$/cm^3 sodium atoms if we assume an aerosol number density of 1000/cm^3. This exceeds typically measured peak values by more than three orders of magnitude. The situation is even worse if we ask for the entire particle to consist of sodium: A total of $5 \cdot 10^9$/cm^3 are needed, far more than available.

We could speculate that the column density of sodium is the more relevant physical quantity in this context because the aerosols are believed to start their nucleation around the cold summer mesopause and then sediment to lower altitudes thereby collecting water molecules and other species, among them sodium. We have estimated the total amount of sodium above 83 km (including various chemical forms and meteoric dust grains) to be $\sim 2 \cdot 10^{10}$/cm^2 (e.g. Hunten *et al.*, 1980; Clemesha *et al.*, 1995). This is to be compared with the sodium content in the aerosol layer observed by DUSTY during flight ECT07. Taking a layer height of 1 km we arrive at $3 \cdot 10^{12}$/cm^2 for a surface monolayer, and at $5 \cdot 10^{14}$/cm^2 to create 1000 aerosols totally consisting of sodium. Thus we again need several orders of magnitude more sodium than the available natural abundances.

We therefore conclude that it is rather unlikely that the aerosols observed during ECT07 consist of pure sodium, at least not if the amount of sodium available in the atmosphere during this flight was anywhere close to standard atmospheric conditions. We note, however, that electron enhancements at NLC heights are rare events. The 'standard' case during PMSE conditions was observed only two days before flight ECT07: In the first salvo during the ECHO campaign the CONE instrument detected an electron biteout at PMSE altitudes. We have applied our model to these measurements and found that the aerosols were negatively charged which is consistent with the assumption that they consist of pure water ice (Lübken *et al.*, 1998).

We conclude that either the measurements are erroneous (which we consider to be unlikely since there are two independent indications for positively charged aerosols, namely the DUSTY measurements, and the electron enhancement detected by CONE), or the amount of sodium in the vicinity of the aerosol layer was far above typical abundances. In order to perform correct model calculations it is necessary to know the abundance and complex refractive index of the particles involved. The optical properties of aerosols which consist of a mixture of various substances are very difficult to model and also difficult to measure in the laboratory under conditions relevant for PMSE and NLC particles.

Regardless of the composition of the aerosol particles our model calculations impose a severe limitation on some of the PMSE theories being presented in the literature. As we have shown in Section 2 the maximum positive charge on the aerosols is approximately +(3–4) e assuming very favorable conditions, namely that the particles consist of pure sodium and that the photoelectrical yield is maximum. This is much smaller than the some hundred positive charges required by some of the PMSE theories like the dust hole scatter theory by Havnes *et al.* (1992) and the opalescence theory by Trakhtengerts (1994).

5. Summary and Conclusion

By applying an aerosol charging model to measurements obtained during the ECHO campaign in 1994 we have demonstrated that the existence of positively charged aerosols can in principle be explained assuming that these aerosols mainly consist of substances allowing for a significant charging by photoemission. Mie calculations of the absorption cross sections of the aerosols have shown that there exists an upper limit of $\sim$4 positive charges as long as the particles are smaller than $\sim$1000 nm. This result is in contrast to earlier theoretical calculations which predicted aerosols with positive charges of more than +100 e (Havnes *et al.*, 1990). Taking into account the photoelectrical properties of metals we have shown that only sodium and potassium have sufficiently low work functions to allow for significant photoemission. We note that the amount of sodium required to form these particles is far above the natural abundances at NLC altitudes. We conclude that the abundance and composition of the aerosols (or their complex refractive index) needs to

be known to perform more sophisticated model calculations. Further experimental observations of aerosol properties at mesospheric heights are required to further elucidate the role of positively charged aerosols in creating NLCs and PMSEs. Such in situ measurements could be triggered by lidar detection of NLCs that require particles of a minimum size of 20–30 nm which is also a necessary though not sufficient condition for the accumulation of positive charge on aerosols.

Acknowledgments. We thank Tom Blix and Ove Havnes for fruitful discussions, and the Andøya Rocket Range (Norway) and the Mobile Raketenbasis of the DLR in Oberpfaffenhofen (Germany) for their support during the ECHO campaign. The rocket flights and the lidar operations were supported by the Bundesministerium für Bildung, Wissenschaft, Forschung und Technologie under grants No. 010E88027 and 50EE94010.

References

Blix, T. A., E. V. Thrane, J. Trøim, and U. P. Hoppe, The role of charged aerosols in connection with noctilucent clouds and polar mesosphere summer echoes, in *Proceedings of the 12th ESA Symposium on European Rocket and Balloon Programmes and Related Research, Lillehammer, Norway*, 1995.

Brasseur, G. and P. C. Simon, Stratospheric chemical and thermal response to long term variability in solar UV-radiance, *J. Geophys. Res.*, **86**, 7343–7362, 1981.

Cho, J. Y. N. and J. Röttger, An updated review of polar mesosphere summer echoes: Observation, theory, and their relationship to noctilucent clouds and subvisible aerosols, *J. Geophys. Res.*, **102**, 2001–2020, 1997.

Clemesha, B. R., D. M. Simonich, H. Takahashi, S. M. L. Melo, and J. M. C. Plane, Experimental evidence for photochemical control of the atmospheric sodium layer, *J. Geophys. Res.*, **100**, 18,909–18,916, 1995.

Ecklund, W. L. and B. B. Balsley, Long-term observations of the Arctic mesosphere with the MST radar at Poker Flat, Alaska, *J. Geophys. Res.*, **86**, 7775–7780, 1981.

Feuerbacher, B. and B. Fitton, Experimental investigation of photoemission from satellite surface materials, *J. Appl. Phys.*, **43**, 1563–1572, 1972.

Fowler, R. H., The analysis of photoelectric sensitivity curves for clean metals at various temperatures, *Phys. Rev.*, **38**, 45–56, 1931.

Havnes, O., U. de Angelis, R. Bingham, C. K. Goertz, G. E. Morfill, and V. Tsytovich, On the role of dust in the summer mesopause, *J. Atmos. Terr. Phys.*, **52**, 637–643, 1990.

Havnes, O., F. Melandsø, C. La Hoz, T. K. Aslaksen, and T. Hartquist, Charged dust in the Earth's mesopause: Effects on radar backscatter, *Phys. Scr.*, **45**, 535–544, 1992.

Havnes, O., J. Trøim, T. Blix, W. Mortensen, L. I. Næsheim, E. Thrane, and T. Tønnesen, First detection of charged dust particles in the Earth's mesosphere, *J. Geophys. Res.*, **101**, 10,839–10,847, 1996.

Hellwege, K. H. and A. M. Hellwege, Eigenschaften der Materie in ihren Aggregatzuständen: Optische Konstanten, *Landolt-Börnstein, Teil*, **8**, 1-1–1-17, 1962.

Hunten, D. M., R. P. Turco, and O. B. Toon, Smoke and dust particles of meteoric origin in the mesosphere and stratosphere, *J. Atmos. Sci.*, **37**, 1342–1357, 1980.

Jensen, E. and G. E. Thomas, Charging of mesospheric particles: Implications of electron density and particle coagulation, *J. Geophys. Res.*, **96**, 18,603–18,615, 1991.

Jesse, O., Untersuchungen über die sogenannten leuchtenden Wolken, *Meteorol Z.*, **8**, 306–308, 1891.

Kurzawa, H. and U. von Zahn, Sodium density and atmospheric temperature in the mesopause region in polar summer, *J. Atmos. Terr. Phys.*, **52**, 981–993, 1990.

Lübken, F.-J., Rocket-borne measurements of small scale structures and turbulence in the upper atmosphere, *Adv. Space Res.*, **17**(11), 25–35, 1996.

Lübken, F.-J., Thermal structure of the arctic summer mesosphere, *J. Geophys. Res.*, **104**, 9135–9149, 1999.

Lübken, F.-J., K. H. Fricke, and M. Langer, Noctilucent clouds and the thermal structure near the arctic mesopause in summer, *J. Geophys. Res.*, **101**, 9489–9508, 1996.

Lübken, F.-J., M. Rapp, T. Blix, and E. Thrane, Microphysical and turbulent measurements of the Schmidt number in the vicinity of polar mesosphere summer echoes, *Geophys. Res. Lett.*, **25**, 893–896, 1998.

Müller, U., A. Schmidt-Ott, and H. Burtscher, Photoelectric quantum yield of free silver particles near threshold, *Z. Phys. B - Condensed Matter*, **73**, 103–106, 1988.

Müller, U., M. Amman, H. Burtscher, and A. Schmidt-Ott, Photoemission from clean and oxygen-covered ultrafine nickel particles, *Phys. Rev. B*, **44**, 8284–8287, 1991.

Natanson, G. L., On the theory of the charging of amicroscopic aerosol particles as a result of capture of gas ions, *Sov. Phys. Tech. Phys.* (engl. Transl.), **30**, 573–588, 1960.

Nussbaumer, V., K. H. Fricke, M. Langer, W. Singer, and U. von Zahn, First simultaneous and common volume observations of noctilucent clouds and polar mesosphere summer echoes by lidar and radar, *J. Geophys. Res.*, **101**, 19,161–19,167, 1996.

Parthasarathy, R., Mesopause dust as a sink for ionization, *J. Geophys. Res.*, **81**, 2392–2396, 1976.

Reid, G. C., Ice particles and electron 'bite-outs' at the summer polar mesopause, *J. Geophys. Res.*, **95**, 13,891–13,896, 1990.

Schmitt-Ott, A., P. Schurtenberger, and H. C. Siegmann, Enormous yield of photoelectrons from small particles, *Phys. Rev. Lett.*, **45**, 1284–1287, 1980.

Thomas, G. E. and C. P. McKay, On the mean particle size and water content of polar mesospheric clouds, *Planet. Space Sci.*, **33**, 1209–1224, 1985.

Trakhtengerts, V. Y., Generation mechanism of polar mesosphere summer echoes, *J. Geophys. Res.*, **99**, 21,083–21,088, 1994.

Turco, R. P., O. B. Toon, R. C. Whitten, R. G. Keesee, and D. Hollenbach, Noctilucent Clouds: Simulation studies of their genesis, properties and global influences, *Planet. Space Sci.*, **3**, 1147–1181, 1982.

Ulwick, J. C., K. D. Baker, M. C. Kelley, B. B. Balsley, and W. L. Ecklund, Comparison of simultaneous MST radar and electron density probe measurements during STATE, *J. Geophys. Res.*, **93**, 6989–7000, 1988.

van de Hulst, H. C., *Light Scattering by Small Particles*, 88ff pp., Dover Publications, Inc., New York, 1981.

von Zahn, U. and J. Höffner, Mesopause temperature profiling by potassium lidar, *Geophys. Res. Lett.*, **23**, 141–144, 1996.

Weast, R. C., *CRC Handbook of Chemistry and Physics*, 59th edition, CRC Press Inc., Florida, 1978.

M. Rapp (e-mail: rapp@physik.uni-bonn.de) and F.-J. Lübken